Sixth International Symposium on Turbulence and Shear Flow Phenomena
Seoul, Korea, 22-24 June 2009

# DETAILED NUMERICAL SIMULATIONS OF A SUPERSONIC INLET-ISOLATOR

**Heeseok Koo**
Department of Aerospace Engineering and Engineering Mechanics,
The University of Texas at Austin
210 E. 24th St. WRW 305A, Austin, Texas, 78712, USA
hkoo@mail.utexas.edu

**Venkatramanan Raman**
Department of Aerospace Engineering and Engineering Mechanics,
The University of Texas at Austin
210 E. 24th St. WRW 305B, Austin, Texas, 78712, USA
v.raman@mail.utexas.edu

## ABSTRACT

An isolator is an important component of dual-mode scramjet engines that separates the combustor from the engine inlet. This flow section contains a time-varying shock-train that adapts to external variations in order to provide a stable flow to the combustion chamber. The goal of this study is to understand the key modeling issues in computing the flow inside an isolator. We develop a large-eddy simulation (LES) based computational tool using a conservative finite difference method. This tool is validated using detailed measurements from an experimental isolator. Several different models, numerical schemes, and computational grids are tested. The shock structure inside the isolator is relatively stable and insensitive to the computational details. All the simulations overpredict the velocity fluctuations in the boundary layer. Further, simulations exhibit boundary layer separation due to shock impingement, a feature absent in the experiments. These studies indicate that current LES modeling practices are inadequate for describing isolator physics.

## INTRODUCTION

Supersonic combustion ramjet engines will play a vital role in the realization of hypersonic flight. Scramjets are relatively simple in design compared to conventional low-speed jet engines but are highly susceptible to flow-induced instabilities. In these engines, the incoming air is compressed through a series of shocks before entering the combustion chamber, where fast mixing with fuel is necessary to ensure stable combustion and engine operation. Dual-mode scramjets provide a practical solution to hypersonic flight by operating at both low and high supersonic Mach numbers. To isolate the effect of flight conditions on the pre-combustion shock structure, a nearly parallel-walled duct is typically used. This flow section, termed an isolator, contains a time-varying shock-train that adapts to external variations in order to provide a stable flow to the combustion chamber. One critical issue is that when the backpressure generated by the combustion process exceeds a critical value, the entire shock structure is dislodged leading to engine unstart. The design objective is to minimize the isolator length while maximizing the range of flow conditions over which the isolator is effective in holding the shock structure. A predictive model for scramjet inlet physics will be a critical step forward in the development of stable hypersonic engines.

The isolator length is typically designed to support the maximum pressure ratio between inlet and exit (Heiser and Pratt, 1994). Usually, this length is determined from empirical correlations (Waltrup and Billig, 1973). While computational fluid dynamics (CFD) studies could potentially aid in isolator design, their accuracy has been limited by the complex shock-boundary layer interaction present in these flows. CFD calculations are typically based on Reynolds averaged Navier-Stokes (RANS) formulations employing low-speed turbulence models with ad-hoc modifications to incorporate the shock-turbulence interaction physics. Consequently, these computations are highly sensitive to the turbulence closures used, and are not reliable for design purposes. Recently, large-eddy simulation (LES) has emerged as a promising alternative for predictive modeling of turbulent flows.

LES-based analysis of shock-turbulence interactions has been mainly studied using the compression ramp as a surrogate problem (Edwards, 2008; Edwards et al., 2008; Loginov et al., 2006; Garnier et al., 2002). The compression ramp problem contains physical processes similar to those found in an isolator, including shock-turbulent boundary layer interaction. Two different issues have to be considered while using LES for such high-speed flow problems: 1) Subfilter closures and 2) numerical implementation. LES resolves only the large scale features of the flow, while the small scale processes are unresolved and have to be modeled. The presence of shock-turbulence interaction and the dominance of near-wall flows provides a challenging modeling problem. Several modeling strategies have been proposed, such as a modified Smagorinsky closure (Garnier et al., 2002), the approximated deconvolution model (Loginov et al., 2006), and the hybrid LES-RANS methodology (Edwards et al., 2008). All these models have proven to be accurate for a range of flow conditions.

The second issue in using LES is the numerical implementation. Shock-capturing schemes are typically upwinded to reduce numerical oscillations but also cause energy dissipation. Since energy conservation and preservation of large-scale fluctuations is central to LES (Mittal and Moin, 1997), a proper of choice of numerical scheme is important. Many different strategies are available (Garnier et al., 2002; Fiorina and Lele, 2007; Cook and Cabot, 2005; Adams and Shariff, 1996; Rizzetta et al., 2001). A common approach is to use energy conserving central schemes along with a filtering scheme to remove the numerical oscillations generated near a shock (Garnier et al., 2002; Fiorina and Lele, 2007). The oscillations also can be suppressed by the addition of a

hyperviscosity term in the vicinity of the shock (Cook and Cabot, 2005). Alternately, a hybrid scheme could be used where the near-shock region is discretized using an upwinded scheme but central schemes are used away from the shock (Adams and Shariff, 1996; Rizzetta et al., 2001). In this case, another parameter to demarcate the near-shock region from the rest of the flow needs to be specified. In spite of these choices, numerical dissipation is an issue in LES of high-speed flows.

With this background, the goal of this work is to assess the relative importance of these two issues in a practical isolator. We use an experimental flow configuration as the basis for our validation (Wagner et al., accepted). By comparing detailed statistics of the flow, the impact of numerical schemes and subfilter models on predictive accuracy will be gauged. The rest of the paper is organized as follows. First, we discuss the numerical implementation and the discretization schemes used. Next, the effect of numerics is discussed. Finally, the effect of subfilter models is discussed.

## LES IMPLEMENTATION AND NUMERICAL DETAILS

In LES, transport equations for filtered variables are solved on a computational grid. For compressible flows, a Favre-filtered field can be written as

$$\widetilde{Q}(\mathbf{x},t) = \frac{1}{\overline{\rho}} \int_{-\infty}^{+\infty} \rho(\mathbf{y},t) Q(\mathbf{y},t) G(\mathbf{y}-\mathbf{x})\, d\mathbf{y}, \tag{1}$$

where $\overline{\rho}$ is the filtered density, and $G$ is the filtering kernel that typically operates over a finite domain. Applying the filtering operation to the continuity and momentum equations, the following filtered transport equations are obtained.

$$\frac{\partial \overline{\rho}}{\partial t} + \nabla \cdot (\overline{\rho}\widetilde{\mathbf{u}}) = 0, \tag{2}$$

and

$$\frac{\partial \overline{\rho}\widetilde{\mathbf{u}}}{\partial t} + \nabla \cdot (\overline{\rho}\widetilde{\mathbf{u}}\widetilde{\mathbf{u}} + \overline{p}\delta - \widetilde{\tau}) + \nabla \cdot \mathcal{M}^u = 0, \tag{3}$$

where $\widetilde{\mathbf{u}}$ is the LES velocity field, $\overline{p}$ is the filtered pressure, and $\tau$ is the viscous stress tensor. $\widetilde{(\cdot)}$ represents filtered LES field.

$$\widetilde{\tau} = \widetilde{\mu}\left(2\widetilde{\mathbf{S}}\right) + \left(\widetilde{\beta} - \frac{2}{3}\widetilde{\mu}\right)(\nabla \cdot \widetilde{\mathbf{u}})\,\delta, \tag{4}$$

where $\widetilde{\mu}$ is the filtered dynamic (shear) viscosity, $\widetilde{\beta}$ is the filtered bulk viscosity, and $\widetilde{\mathbf{S}}$ is the filtered strain rate tensor.

$$\widetilde{\mathbf{S}} = \frac{1}{2}\left(\nabla\widetilde{\mathbf{u}} + (\nabla\widetilde{\mathbf{u}})^T\right). \tag{5}$$

$\mathcal{M}^u$, the subfilter stress that arises from the filtering of the nonlinear convection term, requires modeling. Additionally, a filtered energy equation is solved along with the ideal gas law to close the system. The total energy is defined as follows:

$$e_t = \frac{P}{\rho(\gamma-1)} + \frac{1}{2}(\mathbf{u}\cdot\mathbf{u}), \tag{6}$$

where $\gamma$ is the ratio of specific heats. Only the filtered total energy is solved here. In order to remove additional modeling constraints, the filtered energy is related to the other field variables as follows:

$$\widetilde{e}_t = \frac{\overline{P}}{\overline{\rho}(\gamma-1)} + \frac{1}{2}(\widetilde{\mathbf{u}}\cdot\widetilde{\mathbf{u}}), \tag{7}$$

where the subfilter kinetic energy and the correlation between temperature and the specific heat capacity have been neglected. The transport equation for filtered energy can be written as

$$\frac{\partial \overline{\rho}\widetilde{e}_t}{\partial t} + \nabla \cdot \left[\overline{\rho}\widetilde{e}_t\widetilde{\mathbf{u}} + (\overline{p}\delta - \widetilde{\tau})\cdot\widetilde{\mathbf{u}} - \kappa\nabla\widetilde{T}\right] + \nabla\cdot\mathcal{M}^e = 0, \tag{8}$$

where $k$ is the thermal conductivity, and $\mathcal{M}^e$ represents the sum of the unclosed terms arising from the nonlinear convection term, the pressure-velocity correlation, and the viscous stress-velocity correlation. Only the subfilter turbulent flux due to convection is modeled here.

The subfilter flux arising from the nonlinear convection term is closed using a Smagorinsky type model.

$$\mathcal{M}^u = \overline{\rho}\left(\widetilde{\mathbf{u}\mathbf{u}} - \widetilde{\mathbf{u}}\widetilde{\mathbf{u}}\right) = 2\mu_t\widetilde{\mathbf{S}}, \tag{9}$$

where $\mu_t$ is the eddy viscosity given by

$$\mu_t = C_s\overline{\rho}\Delta^2\mathcal{S}, \tag{10}$$

where $C_s$ is a model coefficient that can be specified as a constant or obtained using a dynamic procedure (Germano et al., 1991). Here, the dynamic procedure is used. $\Delta$ is the filter width and $\mathcal{S}$ is the magnitude of the filtered strain rate tensor. A similar approach is used to model $\mathcal{M}^e$ (Germano et al., 1991).

In this study, we use a conservative finite difference (C-FD) approach as the basic numerical discretization scheme. It is well known that the conservative approaches such as finite volume and C-FD are superior to conventional finite difference methods for shock-containing problems due to the ability to estimate shock speed correctly and satisfy the Rankine-Hugoniot relation across discontinuities (Leveque, 2002).

For a one-dimensional C-FD formulation, the flow equations (Eq. 2, 3, and 8) are written as

$$\frac{\partial \widehat{Q}}{\partial t} + \frac{\partial F_i}{\partial x_i} = 0, \tag{11}$$

where $\widehat{Q}$ is a cell-averaged conservative variable, and $F_i$ is the flux in the $i$-th direction.

$$\widehat{Q_i} = \frac{1}{\Delta_i}\int_{i-\frac{1}{2}}^{i+\frac{1}{2}} Q(x)dx, \tag{12}$$

where $\Delta_i$ is the grid spacing in the $i$-th direction. Eq. 11 can be rewritten as (Merriman, 2003)

$$\frac{\partial \widehat{Q}}{\partial t} + \frac{G_{i+\frac{1}{2}} - G_{i-\frac{1}{2}}}{\Delta_i} = 0, \tag{13}$$

where

$$F(x_i) = \frac{\int_{x_i-\frac{\Delta_i}{2}}^{x_i+\frac{\Delta_i}{2}} G(x_i)dx_i}{\Delta_i} \tag{14}$$

$G$ at the intermediate nodes can be approximated using higher-order finite volume compact schemes (Pirozzoli, 2002). Thus, the primitive variables and their gradients are first reconstructed at the intermediate nodes. The cell-face fluxes are then evaluated based on these node values. Here, a 6-th order Padé scheme is used for this reconstruction. The boundaries are handled using one-sided or modified Padé schemes (Kobayashi, 1999; Piller and Stalio, 2004). Extension of this approach to higher dimensions is straightforward (Pirozzoli, 2002).

In the current study, two different numerical discretization strategies are used to evolve the filtered equations (Eq. 2, 3, and 8) in the C-FD context. The hyperviscosity-based approach is discussed first. Then, the weighted essentially non-oscillatory (WENO) scheme is discussed. It

should be noted that the numerical schemes themselves provide dissipation, and can sometimes act as a subfilter model. For this reason, the nature of the subfilter model used depends on the numerical scheme used. When the numerical schemes are discussed, the corresponding subfilter modeling approach is also explained.

The hyperviscosity approach, as the name suggests, adds a shock-based viscosity to the molecular viscosity, thereby providing additional dissipation near the shock. In this model, the coefficients $\mu$, $\beta$, and $k$ in Eq. 4 and 8 are modified as $\mu = \mu_f + \mu^*$, $\beta = \beta_f + \beta^*$, $\kappa = \kappa_f + \kappa^*$, where $f$ subscripts and asterisks denote fluid and artificial coefficients (Fiorina and Lele, 2007). For air, $\beta_f$ is negligible. The artificial viscosity and diffusivity in a generalized coordinate system are given by,

$$\mu^* = C_\mu \rho \overline{\sum_{l=1}^{3} \left[ \sum_{m=1}^{3} \left( \frac{\partial \xi_l}{\partial x_m} \right)^2 \right]^{r/2} \left| \frac{\partial^r S}{\partial \xi_l^r} \right| \Delta_l^{r+2}}, \qquad (15)$$

$$\beta^* = C_\beta \rho \overline{\sum_{l=1}^{3} \left[ \sum_{m=1}^{3} \left( \frac{\partial \xi_l}{\partial x_m} \right)^2 \right]^{r/2} \left| \frac{\partial^r S}{\partial \xi_l^r} \right| \Delta_l^{r+2}}, \qquad (16)$$

$$\kappa^* = C_\kappa \frac{\rho a}{T} \overline{\sum_{l=1}^{3} \left[ \sum_{m=1}^{3} \left( \frac{\partial \xi_l}{\partial x_m} \right)^2 \right]^{r/2} \left| \frac{\partial^r e}{\partial \xi_l^r} \right| \Delta_l^{r+1}}, \qquad (17)$$

where $\xi_l$ refers to generalized coordinates $\xi$, $\eta$ and $\zeta$ and $x_m$ refers to $x$, $y$, and $z$ when subscript $l$ and $m$ indicate spatial directions. $\Delta_l$ is grid spacing in physical space in the $\xi_l$ direction, and $a$ is local speed of sound. In this study, $r$ is fixed to 4, and user specified constants are set to $C_\mu = 0.002$, $C_\beta = 1$, $C_\kappa = 0.01$ (Cook and Cabot, 2005; Kawai and Lele, 2008b). For wall bounded problems, the coefficients are smoothly damped using the Van Driest wall damping function (Kawai and Lele, 2008a).

The overbar ($\bar{\cdot}$) in the above equations indicates a filtering operation to reduce large fluctuations in the hyperviscosity term. A Gaussian filter is used for this purpose (Cook and Cabot, 2005).

$$\overline{f_i} = \frac{3565}{10368} f_i + \frac{3091}{12960} (f_{i-1} + f_{i+1}) + \frac{1997}{25920} (f_{i-2} + f_{i+2}) + \frac{149}{12960} (f_{i-3} + f_{i+3}) + \frac{107}{103680} (f_{i-4} + f_{i+4}) \qquad (18)$$

The hyperviscosity mimics a subfilter turbulent flux model and removes energy at the smallest resolved scale. Consequently, no explicit turbulence closure is used with the hyperviscosity approach.

Unlike the hyperviscosity approach that achieves stability by adding artificial dissipation, the WENO approach provides stability by employing a variable stencil for computing the convective terms (Jiang and Shu, 1996). Here, the numerical flux is calculated through the weighted sum of the exact flux values at adjacent nodes. While providing numerical stability, this weighting process also tries to ensure that dissipation of physical fluctuations is minimized. In this work, a standard 5-th order WENO (Jiang and Shu, 1996) is implemented along with a 4-th order finite difference method for the viscous terms. The dynamic Smagorinsky model is used to close the subfilter flux in this case.

The discretized equations for both schemes are integrated in time using a third-order Runge-Kutta method. When used with the hyperviscosity approach, the conservative variables are filtered at each Runge-Kutta step (Kawai and Lele, 2008b) using an 8th order compact filter (Gaitonde and Visbal, 2000).

## FLOW CONFIGURATION

The flow configuration is based on the scramjet inlet experiment performed at the University of Texas (Wagner et al., accepted). A Mach 5 flow is compressed in a constant area rectangular duct with a 6-degree inlet ramp. The boundary layer thickness at the inlet is roughly 75% of the isolator height. The width of the isolator is equal to the height. Using physical properties of air, the Reynolds number based on boundary layer thickness is $1.01 \times 10^6$. Molecular viscosity of air follows Sutherland's formula. A number of simulations are carried out to understand the impact of the grid resolution, the subfilter model, and the numerical discretization method. Two grid resolutions are considered, with the coarse mesh consisting of 256×128×32 grid points and the fine mesh consisting of 512×256×64 grid points. The grid spacing is uniform in the stream- and span-wise directions, and clustered in the wall-normal direction. The $y^+$ value of the first grid point is aroung 5.2 for the lower wall, and 16.7 for the upper wall. Note that the boundary layer on the upper wall is much thinner than the lower-wall boundary layer. The computational grid is shown in Fig. 1. A separate boundary layer simulation was carried out to obtain the inflow conditions. Planes of velocity, density, and temperature data from this simulation were used as the inflow boundary condition. The isolator is assumed to be periodic in the spanwise direction, which is reasonable given that sidewall compression and boundary layers were unimportant in the experimental configuration (Wagner et al., accepted). Navier-Stokes characteristic non-reflecting boundary conditions are used for the outflow.

## RESULTS AND DISCUSSION

The baseline simulation is performed on the coarse mesh using the hyperviscosity method. Figure 1 shows the computational grid, as well as instantaneous density gradient and pressure plots. The pressure contours are necessary to identify the shocks, since the density gradients are affected by the compressible boundary layer as well. The pressure contours indicate the presence of a series of oblique shocks, with some distortion due to the refracted waves from the boundary layer. This flow condition is fully supersonic and provides only weak compression. The density gradient contours show the interaction of the turbulent boundary layer with the oblique shocks. The first interaction on the lower wall increases the thickness of the boundary layer and introduces additional flow structures. It can also be seen that the third reflected shock on the lower wall is very weak and is quickly dissipated by the boundary layer.

Figures 2 and 3 compare experimental data (Wagner et al., accepted) with the baseline simulation. The mean velocity contour plots (Fig. 2) show several interesting features. The simulations predict a small separation region on the top wall due to the reflected shock. The stream-wise velocity contains a low-velocity region on the top wall while the normal component shows mean velocity moving away from the wall. The experimental data does not show any separation, indicating that this effect is an artifact of the computational method. The presence of this separation region weakens the shock reflection, and the third reflection on the bottom wall is very weak compared to the other two reflections. Further, this separation region changes the reflection angle, and the third reflection is pushed downstream compared to the experiments. Figure 3 shows the root mean square (RMS) of velocity components from experiment and simulation. The fluctuations in the boundary layer are always overpredicted

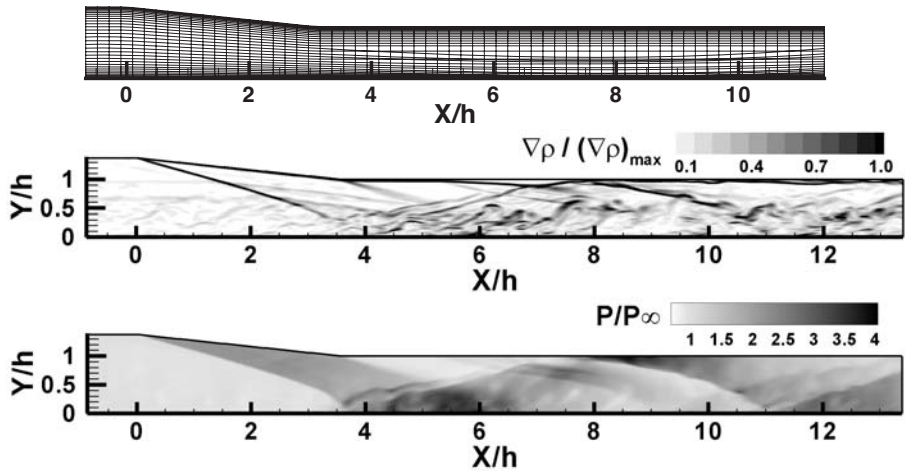


Figure 1: (Top) Computational grid with every eighth-point plotted. (Middle) Instantaneous $\nabla\rho$ non-dimensionalized by maximum plotted value and (bottom) pressure contour for hyperviscosity in coarse grid case.

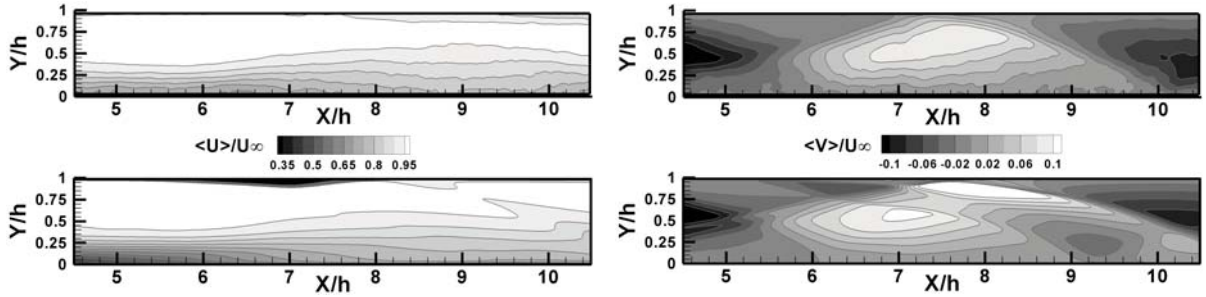


(a) (b)

Figure 2: Mean streamwise (a) and normal (b) velocity contours for experiment (up) and numerical results using hyperviscosity method (down).

in the simulations. It is noted that similar results were obtained by (Boles et al., 2009) using the hybrid RANS/LES approach.

Based on these results, a series of model and algorithmic modifications were considered in an effort to understand the sensitivity of the results to the computational method. In the first study, the numerical discretization scheme was changed from the hyperviscosity approach to the WENO scheme. The Padé scheme used in the hyperviscosity approach has very good spectral properties (Lele, 1992). The computations here support this conclusion, with the WENO calculation being far more dissipative than the hyperviscosity approach. The WENO computations on a finer grid (Fig. 4) exhibited more coherent structures in the boundary layer, and compared well with the coarse grid hyperviscosity solution. This result demonstrated that grid anisotropy impacts the WENO scheme more than the compact Padé scheme.

However, this added accuracy of the hyperviscosity approach comes at an increased computational cost. The computational time-step scales as the inverse square of viscosity, and the addition of artificial viscosity adversely impacts the time-step. This additional viscosity is based on a higher-order derivative of the strain rate, and becomes very large in the vicinity of the shock or the walls. In this work, a damping function is used to limit this viscosity in the near-wall region. Further, the coefficient that controls bulk viscosity ($C_\beta$ in Eq. 16) is reduced to 0.1. This latter change was tested on canonical problems and was found to provide stable solutions. In spite of these changes, the computational cost of the hyperviscosity approach was five times more than the WENO approach for identical computational grids.

The subfilter model for turbulent flux is an important component of the simulations. Wall-bounded flows, especially those containing shocks, pose a tremendous modeling challenge. The objective of this study was simply to understand the sensitivity of the simulations to commonly used subfilter models. Simulations using the constant coefficient and dynamic version of the Smagorinsky model were conducted. In addition, a simulation with no subfilter model was also performed. Surprisingly, none of these changes produced any marked change in the simulation results. For instance, Fig. 5 shows the wall pressure from these simulations compared with the experimental data. This lack of sensitivity could be due to two reasons. First, the dominant error in this simulation could arise from some other model or boundary condition. Hence, the smaller error introduced by the subfilter models may not be noticeable in these comparisons. Second, the sole purpose of the models tested here is to provide energy dissipation. However, it is well-known that the structure of the near-wall flow is far more complex with aniostropic energy production and transport. If these processes are dominant, then the error introduced by changing the dissipative part of the model will not provide any appreciable difference. These differences clearly point out the need for more detailed research on shock boundary layer

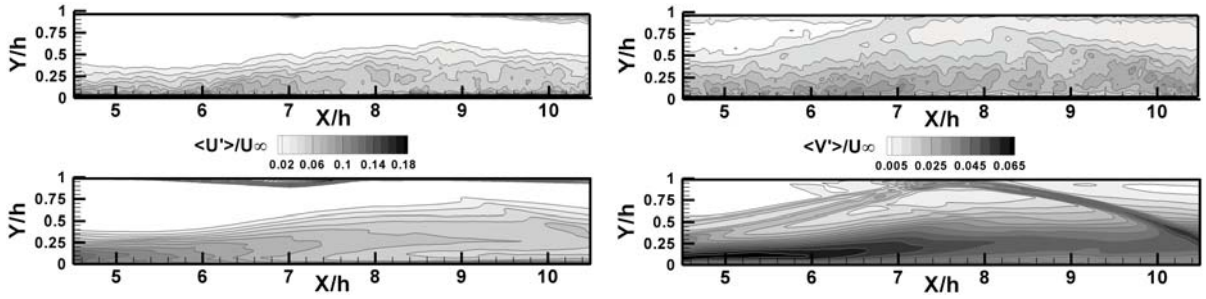


Figure 3: Mean standard deviation of streamwise (a) and normal (b) velocity components for experiment (up) and numerical results using hyperviscosity method (down).

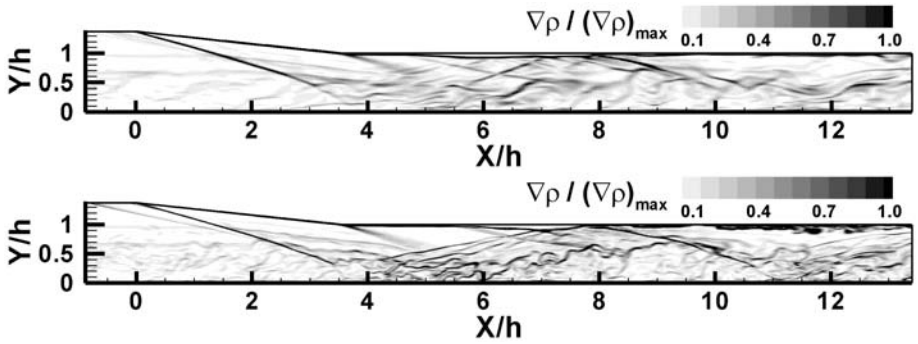


Figure 4: Instantaneous $\Delta\rho$ non-dimensionalized by maximum plotted value of coarse (up) and fine (down) grid systems using WENO with dynamic Smagorinsky sub-grid scale model.

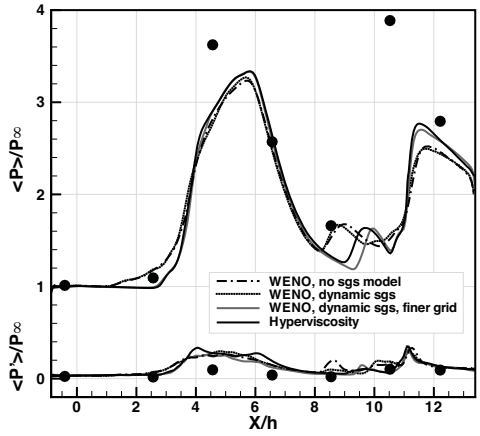


Figure 5: Mean wall pressure and its standard deviation for experiment (dot) and numerical results from various cases.

interaction.

## CONCLUSION

A Mach 5 scramjet inlet-isolator configuration was computed using detailed numerical simulations. The confined supersonic flow in this geometry exhibits complex shock structures that interact with the highly compressible boundary layer. Comparison with experimental data shows that although the shock structure is captured well, the time-averaged velocity and RMS velocity fields are not accuately predicted. Simulations overpredict the RMS fluctuations in the boundary layer, and also exhibit strong boundary layer separation that is absent in the experiments. Interestingly, these results were relatively insensitive to the discretization scheme and the subfilter model used. While grid refinement does provide more structures in the turbulent boundary layer, the time-averaged results still do not agree closely with experiments. This indicated that the dominant source of error has not been uncovered yet.

## ACKNOWLEDGEMENTS

This work was supported through a cooperative grant from NASA (Grant no. NNX08AB41A), with Dr. Andrew Norris as the technical monitor. Computational time from the Texas Advanced Computing Center (TACC) is gratefully acknowledged.

## REFERENCES

*

Adams, N. A., and Shariff, K., 1996, "A high-resolution hybrid compact-eno scheme for shock-turbulence interaction problems," *Journal of Computational Physics*, Vol. 127, pp. 27-51.

Boles, J. A., Choi, J., and Edwards., J. R., 2009, "Simulations of high-speed internal flows using les/rans models," In *47th AIAA Aerospace Sciences Meeting and Exhibit*, No. 2009-1324.

Cook, A., and Cabot, W., 2005, "Hyperviscosity for shock-turbulence interactions," *Journal of Computational Physics*, Vol. 203, pp. 379-385.

Edwards, J. R., 2008, "Numerical simulations of shock / boundary layer interactions using time-dependent modeling techniques - a survey of recent results," In *46th AIAA Aerospace Sciences Meeting and Exhibit*, No. 2008-525.

Edwards, J. R., Choi, J., and Boles, J. A., 2008, "Large-eddy/reynolds-averaged navier-stokes simulation of a mach 5 compression-corner interaction," *AIAA Journal*, Vol. 46(4), pp. 977-991.

Fiorina, B., and Lele, S., 2007, "An artificial nonlinear diffusivity method for supersonic reacting flows with shocks," *Journal of Computational Physics*, Vol. 222, pp. 246-264.

Gaitonde, D., and Visbal, M., 2000, "Pade-type higher-order boundary filters for the navier-stokes equations," *AIAA Journal*, Vol. 38(11), pp. 2103-2112.

Garnier, E., Sagaut, P., and Deville, M., 2002, "Large eddy simulation of shock/boundary-layer interaction," *AIAA Journal*, Vol. 40(10), pp. 1935-1944.

Germano, M., Piomelli, U., Moin, P., and Cabot, W., 1991 "A dynamic subgrid-scale eddy viscosity model," *Physics of fluids A - Fluid dynamics*, Vol. 3(7), pp. 1760-1765.

Heiser, W. H., and Pratt, D. T., 1994, *Hypersonic Airbreathing Propulsion*, published by AIAA.

Jiang, G.-S., and Shu, C.-W., 1996, "Efficient implementation of weighted eno schemes," *Journal of Computational Physics*, Vol. 126, pp. 202-228.

Kawai, S., and Lele, S., 2008a, "Large-eddy simulation of jet mixing in a supersonic turbulent crossflow," *Center for Turbulence Research Annual Research Briefs*, pp. 139-151.

Kawai, S. and Lele, S., 2008b, "Localized artificial diffusivity scheme for discontinuity capturing curvilinear meshes," *Journal of Computational Physics*, Vol. 227(22) pp. 9498-9526.

Kobayashi, M., 1999, "On a class of pade finite volume method," *Journal of Computational Physics*, Vol. 156 pp. 137-180.

Lele, S., 1992, "Compact finite difference schemes with spectral-like resolution," *Journal of Computational Physics*, Vol. 103 pp. 16-42.

Leveque, R. J., 2002, *Finite volume methods for hyperbolic problems*, published by Cambridge University Press.

Loginov, M. S., Adams, N. A., and Zheltovodov, A. A., 2006, "Large-eddy simulation of shock-wave/turbulent-boundary-layer interaction," *Journal of Fluid Mechanics*, Vol. 565, pp. 135-169.

Merriman, B., 2003, "Understanding the shu-osher conservative finite difference form," *Journal of Scientific Computing*, Vol. 19, pp. 309-322.

Mittal, R., and Moin, P., 1997 "Suitability of upwind-based finite difference schemes for large-eddy simulation of turbulent flows," *AIAA Journal*, Vol. 35(8), pp. 1415-1417.

Piller, M., and Stalio, E., 2004, "Finite-volume compact schemes on staggered grids," *Journal of Computational Physics*, Vol. 197, pp. 299-340.

Pirozzoli, S., 2002, "Conservative hybrid compact-weno schemes for shock-turbulence interaction," *Journal of Computational Physics*, Vol. 178, pp. 81-117.

Rizzetta, D. P., Visbal, M. R., and Gaitonde, D. V., 2001, "Large-eddy simulation of supersonic compression-ramp flow by high-order method," *AIAA Journal*, Vol. 39(12), pp. 2283-2292.

Wagner, J. L., Yuceil, K. B., Valdivia, A., Clemens, N. T., and Dolling, D. S., accepted, "Experimental investigation of unstart in an inlet/isolator model in mach 5 flow," *AIAA Journal*.

Waltrup, P. J., and Billig, F. S., 1973, "Prediction of precombustion wall pressure distributions in scramjet engines," *Journal of Spacecraft and Rocket*, Vol. 10(9), pp. 620-622.